

## Geo-referencing images of wide-angle optical systems

© T.E. Syrenova,<sup>1</sup> A.B. Beletsky,<sup>1</sup> R.V. Vasilyev<sup>1,2</sup>

<sup>1</sup> Institute of solar-terrestrial physics of Siberian branch of Russian academy of sciences,  
664033 Irkutsk, Russia

<sup>2</sup> Irkutsk State University,

664003 Irkutsk, Russia

e-mail: angata@mail.iszf.irk.ru

Received June 7, 2021

Revised July 20, 2021

Accepted August 10, 2021

A technique is described for referecing images of wide-angle optical systems intended for registration own radiation of the Earth's atmosphere, to geographic coordinates. The technique is based on an automatic procedure for the stars emphasizing and identification in the frames and subsequent georeferencing. An example of the technique use for calculating the characteristics of a long-lived meteor trail based on observation data of two spatially separated wide-angle optical systems is shown.

**Keywords:** Geo-referencing, all-sky camera, star identification, atmospheric emission, long-lasting trail.

DOI: 10.21883/TP.2022.15.55269.172-21

### Introduction

When observing the Earth's upper atmosphere with optical instruments, a geographic reference is necessary to estimate the altitude and other spatial parameters of the observed events. To do this, you need to know the exact correspondence of the frame pixels of optical systems to the Earth coordinates. This can be done by linking to objects with known coordinates, such as stars. Currently, applications have been developed to identify the stars obtained with optical instruments used in astronomical observations, e.g. Izmccd [1], Astrometry.net [2]. But these applications do not work for wide-angle optical systems. Wide-angle cameras, designed to record the spatial distribution of the intensity of atmospheric emissions, are a fairly convenient and accessible ground-based means of recording various events occurring in the Earth's upper atmosphere. The task of selecting and identifying stars in the frame is complicated by the fact that the above optical systems record optical radiation in a narrow spectral range. Since rather powerful atmospheric emissions are emitted in the recorded bands, the ratio of the star intensity in this spectral range to the background (to which the atmospheric emission makes the main contribution), is significantly lower than the same ratio in the data of optical systems with a wide spectral recorded range.

In this case, the possibility of using two or more instruments separated by some distance allows to determine the spatial parameters of the observed events [3–5]. Optical observations using spatially spaced instruments were carried out as early as the early 20th century to most accurately determine the spatial characteristics of meteors, auroras or silvery clouds [6–10]. The work [10] describes an original method, based on the analysis of stereo images, for obtaining the average height and measuring the main

parameters of acoustic-gravity waves in the mesosphere, such as horizontal wavelength, time period and vertical amplitude of waveforms. In addition, studies of luminous formations resulting from the operation of heating stands were performed using optical instruments. The artificial airglow was recorded at two spaced points by all-sky cameras at wavelengths of 630 and 557.7 nm. As a result, images of luminous regions were obtained, which made it possible to determine the spatial parameters of the formations, their relationship with the parameters of the powerful radio wave, to estimate the amount of additional ionization caused by the heating stand [11,12] by the stereoscopic method.

### 1. Description of methodology

In image processing, an important aspect is the exact matching of pixel coordinates and image projections [13]. At the same time, there is significant image distortion in the frames obtained using optical systems with „fisheye“ lenses. In addition to distortions due to optical aberrations, decentralization — the difference in the position of the true zenith and the center of the image — can also make an error in determining coordinates. Quite a number of works are devoted to this issue, which include camera calibration using different models in order to get rid of the mentioned distortions, e.g. [14–18].

The methodology proposed in this paper includes geometric camera calibration with the selection of coefficients that take into account the aberrations described above, as well as finding geographic coordinates for each pixel of the wide-angle camera image for any height.

Georeferencing was performed using reference points identified as stars by the automatic algorithm. The first step of the star extraction algorithm is the removal of noise

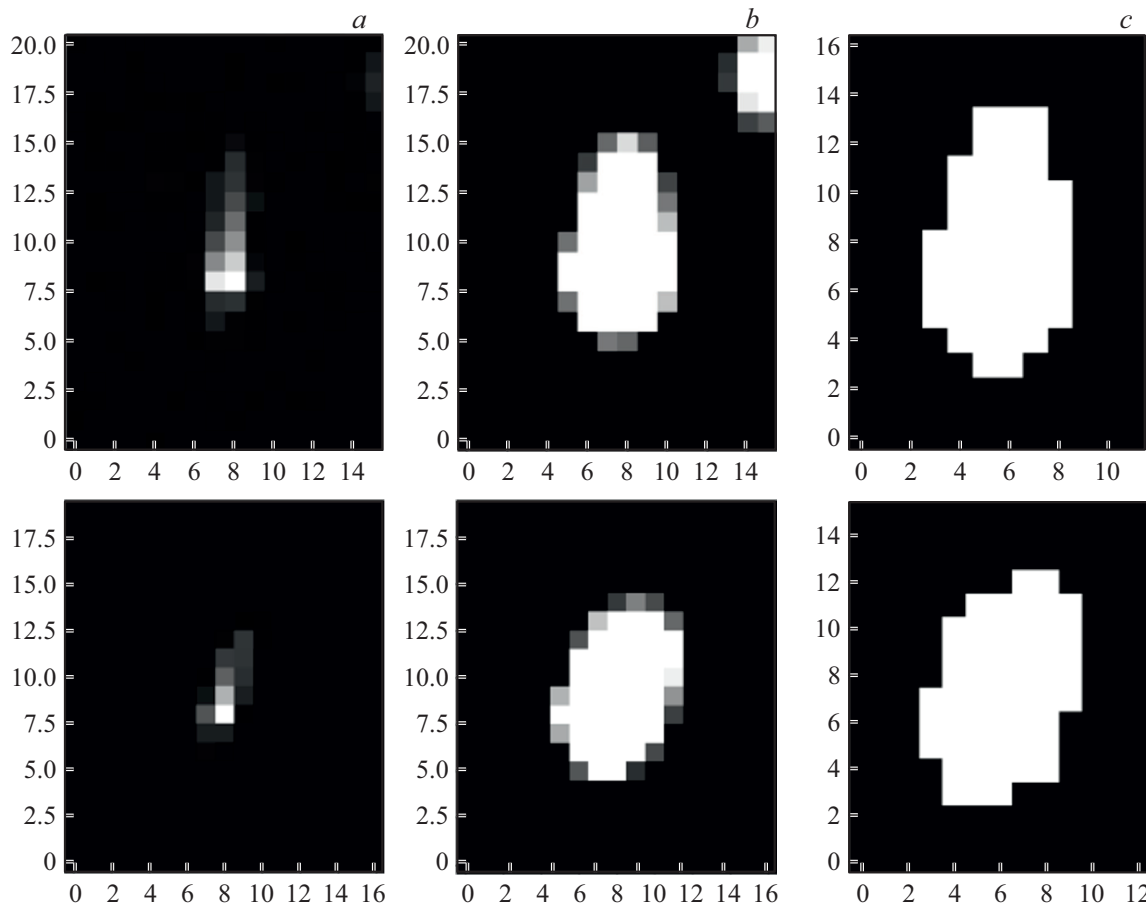


**Figure 1.** Portions of the KEO Sentinel Optical System frame obtained on December 3, 2016 at 16:50 UT without processing (*a*), contrasted (*b*) and a group of pixels identified by the algorithm as a star image (*c*).

pixels. To do this, the image is aligned by removing the low-frequency trend — from the original frame, a frame smoothed by the Gaussian filter [19] over twenty pixels is taken. Then, single pixels with intensity values exceeding a certain threshold calculated as follows are selected:

$$I_{\text{noise}} = I_{\text{mean}} K_{\text{noise}}.$$

The  $K_{\text{noise}}$  factor is chosen empirically for a particular optical system. For KEO Sentinel  $K_{\text{noise}}$  is two. Neighboring pixels exceeding the threshold value are combined into polygons. A pixel is defined as a noise one if the number of pixels in the polygon is maximum one. When a pixel is defined as a noise pixel, it is assigned an average value of the surrounding pixels.

The image is then contrasted using an adaptive histogram equalization procedure with contrast limitation. After that, we search for polygons of related pixels with values exceeding the threshold  $I_{\text{star}}$  and the number of pixels in the group more than  $N_{\text{min}}$  and less than  $N_{\text{max}}$ . The values  $N_{\text{min}}$  and  $N_{\text{max}}$  are chosen empirically for a particular optical system.  $N_{\text{min}}$  allows you to limit the stellar magnitude of the found pixel groups. For example, for the KEO Sentinel optical system,  $N_{\text{min}} = 5$  allows you to select groups of pixels with magnitudes brighter than three. Selecting  $N_{\text{max}}$

allows you to cut off large bright objects such as the moon, moonlit clouds, glare on the dome, etc. For KEO Sentinel  $N_{\text{max}} = 100$ . Fig. 1 shows portions of the camera frame with groups of pixels defined by the algorithm as the star image (*c*), the same portions in the original frame (*a*) and after the contrasting procedure (*b*).

For each object, the azimuth and elevation in the horizontal coordinate system centered at the camera location and the corresponding horizontal and vertical image pixel numbers were compared.

Next, expressions were used to compare the coordinates of a pixel in the image with the corresponding elevation angle and azimuth:

$$\phi(x, y) = \tan^{-1} \left( \frac{y - y_0}{x - x_0} \right) + \phi_0, \quad (1)$$

$$\theta(x, y) = ar^2 + br + c, \quad (2)$$

$$r = \sqrt{(x - x_0)^2 + (y - y_0)^2}. \quad (3)$$

Expression (1) defines the azimuth angle, taking into account the arbitrary rotation of the camera by the angle  $\phi_0$ , where  $x, y$  — pixel coordinates in the image,  $x_0, y_0$  — position of the true zenith in these coordinates.

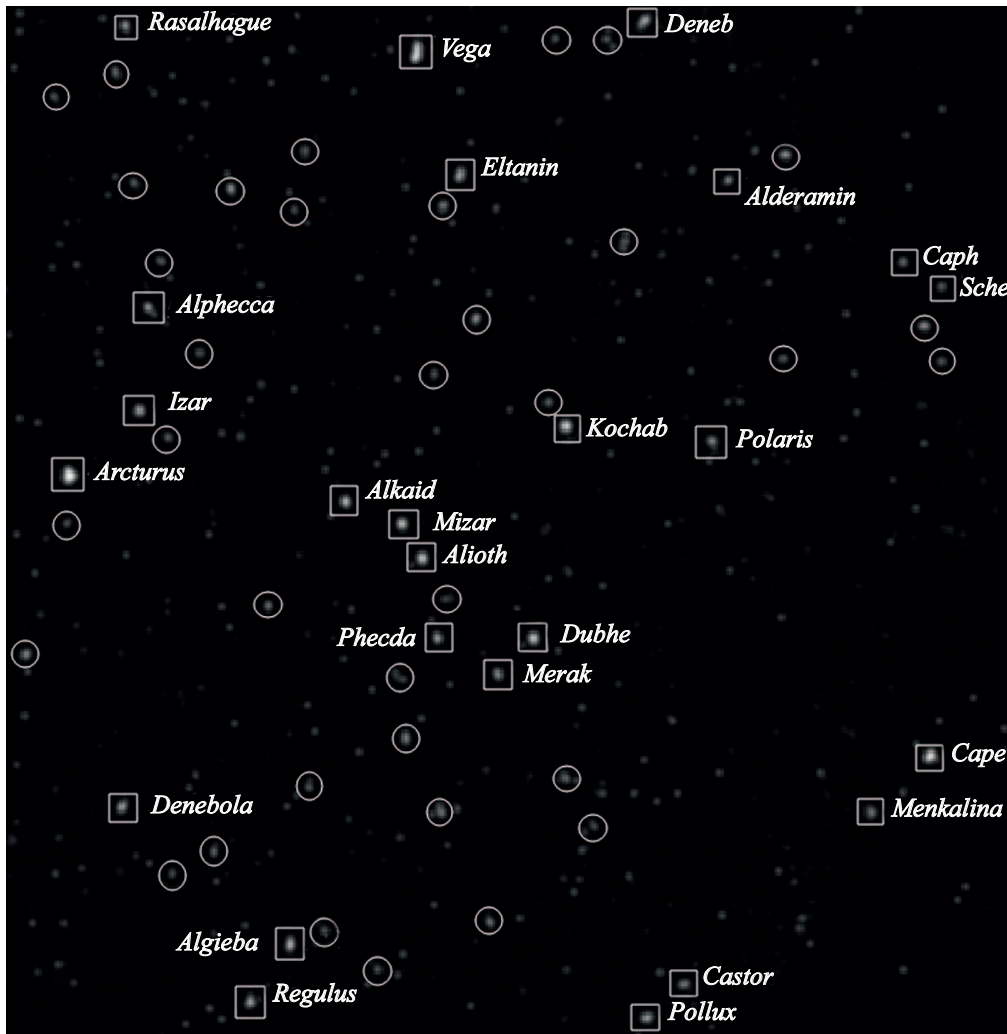


**Figure 2.** Example of the star identification algorithm. A part of the frame of the KEO Sentinel optical system, registered on April 12, 2018, is shown. The circles indicate the areas of the frame identified as stars, the squares — those matched with the star catalog.

Equation (2) defines the zenith angular distance of a pixel, which is conveniently written using the distance between an arbitrary pixel and the true zenith on the matrix (3). The given dependence is quadratic with respect to distance (3) with constant coefficients  $a$ ,  $b$  and  $c$ . Similar dependencies together with the exponential representation for wide-angle cameras were used in [20,21]. Then in subsequent works [22], it was shown that the quadratic dependence is more accurate and contains the smallest errors. The relation between coordinates (1)–(3) can also be represented in the complex form

$$z = x + iy = \theta(x, y) \exp^{i\varphi(x, y)}, \tag{4}$$

where the dependences  $\theta(x, y)$  and  $\varphi(x, y)$  are defined by expressions (1)–(3). Using the reference coordinates of the stars in the horizontal system and their respective positions on the camera matrix, the constant coefficients in (1)–(3) can be found by the method of least squares (MSS), using (4) as a model function. The minimization problem of MNC using (4) was solved using the

Levenberg–Marquardt [23] algorithm. As an error function, we used the difference modulus (5) for the elevation and azimuth of the object from the PyEphem [24] catalog and for the horizontal coordinates obtained from the pixel coordinates corresponding to the center of the object in the camera image

$$S = \sum_{n=0}^M |\theta_n e^{i\varphi_n} - \theta(x_n, y_n) e^{i\varphi(x_n, y_n)}| \tag{5}$$

for the position angle and azimuth of the  $n$ th object from the star catalog, and its corresponding coordinates in the image.

Fig. 2 shows part of the frame of the KEO Sentinel optical system on April 12, 2018. A total of 29 stars were identified in the full frame, matching the stellar catalog, with brightness ranging from  $-1.44$  to  $1.98$ .

Fig. 3 shows the trajectories of the stars identified in the KEO Sentinel frame on December 3, 2016.

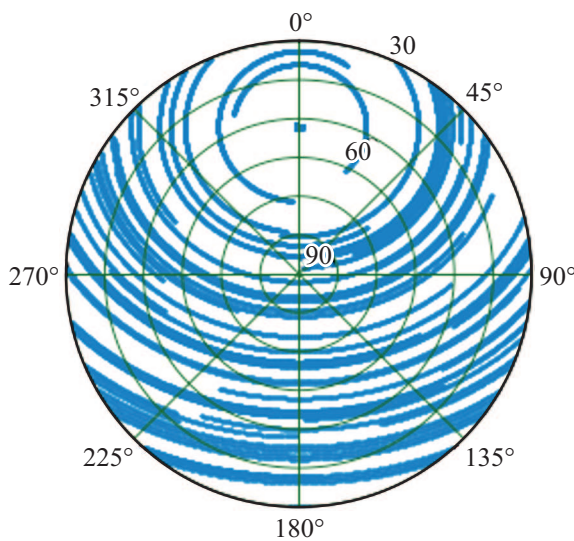


**Figure 3.** Example of the trajectories of the stars identified in the December 3, 2016 frame

The following parameter values of expressions (2)–(4) were obtained for the KEO Sentinel optical system frames for December 3, 2016:  $a = 0.00000089$ ,  $b = -0.29$ ,  $c = 90.55$ ,  $\phi = 264.30$ ,  $x_0 = 256.77$ ,  $y_0 = 265.50$ . Fig. 4 shows the errors in the position angles and azimuths of the stars identified in the frames of December 3, 2016. For the other parameters, the standard deviations are also quite small, indicating that the proposed algorithm is quite stable.

Next, you need to come to a common coordinate system for the two cameras. It is most convenient to go to the geographic coordinates of camera image projections on the Earth surface for further camera operation and comparison of the obtained data with the results of observations of other instruments (optical and radio-physical). The position of each pixel of the image using expressions (2)–(4) and the obtained constant coefficients can be converted into horizontal coordinates. For most geophysical tasks of observing parameters of the upper atmosphere it is not necessary to use a geoid as a model of the Earth. Then, by the solution of the direct geodesic problem on the ball [25] the geographic coordinates of the projection of the image from some height on the Earth’s surface can be found. The inputs are the latitude and longitude of the observation point, the azimuth  $\phi$ , the elevation angle  $\theta$  and the estimated altitude  $h$ , and the spherical distance  $\sigma$  from the camera location to the projected point is calculated by the formula

$$\sigma = 180 - (90 + \theta) - \arcsin\left(\frac{R_E \sin(90 + \theta)}{R_E + h}\right), \quad (6)$$

where  $R_E$  — the radius of the Earth.

The latitude of the projected point is determined by the formula

$$\varphi_2 = \arcsin(\sin \varphi_1 \cos \sigma + \cos \varphi_1 \sin \sigma \cos \phi_0), \quad (7)$$

where  $\varphi_1$  — geographic latitude of the observation point,  $\phi_0$  — azimuth.

The formula for finding the longitude  $\lambda_2$  of a projected point

$$\lambda_2 = \lambda_1 + \arctg\left(\frac{\sin \sigma \frac{\sin \alpha_1}{\cos \varphi_1} \cos \sigma - \sin \varphi_1 \sin \sigma \cos \alpha_1}{\cos \varphi_1}\right), \quad (8)$$

where  $\lambda_1$  — the geographic longitude of the observation point.

## 2. Result of the proposed methodology

The methodology presented in this paper was tested on the example of a long-lived meteor trace (LLMT), which was observed simultaneously by two wide-angle cameras, spatially spaced at a distance of about 150 km. The first camera — the KEO Sentinel all-sky camera — is located at the Geophysical Observatory (GPO) of the ISTP SB RAS SB RAS, near Tory village ( $51^\circ 48' N$ ,  $103^\circ 04' E$ , elevation 670 m) and is designed to record the spatial pattern of 630 nm (180–300 km luminance height) emission intensity. Viewing direction — zenith, field of view  $145^\circ$ , exposure time 30–60 s. The half-width of the interference filter  $\sim 2$  nm [26]. The second Allsky-340 wide-angle color camera manufactured by SBIG is located at the Sayan Solar Observatory of the ISTP SB RAS SB RAS, near the Mondy village ( $51^\circ 40' N$ ,  $100^\circ 59' E$ , elevation 1992 m).

The meteor trace of duration  $\sim 35$ –40 min was recorded after the meteoroid explosion on 11/18/2017 almost simultaneously, at 22.23.19 UT. The characteristics of this meteor trace [27–29] have previously been investigated. The spatial and kinematic characteristics of the meteor trace were determined and the peculiarities of its evolution were revealed in work [29]. Values of heights of ignition and extinction of the meteor itself were in the range 75–120 km, assessment of the brightness of the meteor gives the value of the absolute stellar magnitude of about 7.3 m. It is shown that the propagation of all parts of the long-lived meteor trace occurs in the same plane at an altitude of about 90 km at a speed of about 320 m/s.

The methodology presented in this paper was used to build projections of images of the meteor explosion and the propagating trace on the Earth’s surface from the data of the two above-described cameras. Using two cameras allows you to build a three-dimensional image of the object. For this purpose, a set of projections in a certain range of heights was created, and the projections built using data from different cameras were compared. If the geographic coordinates of a part of a meteor or LLMT in a given set coincide at a certain altitude, it means that this part of the object is concentrated at that altitude. By the stereoscopic method of projection analysis, it was determined that the meteor lights up at an altitude of about 111 km and goes out at an altitude of 78 km, and the total track length is about 38 km (Fig. 5). In this case, the error of heights determining is within  $\pm 1.2$  km.

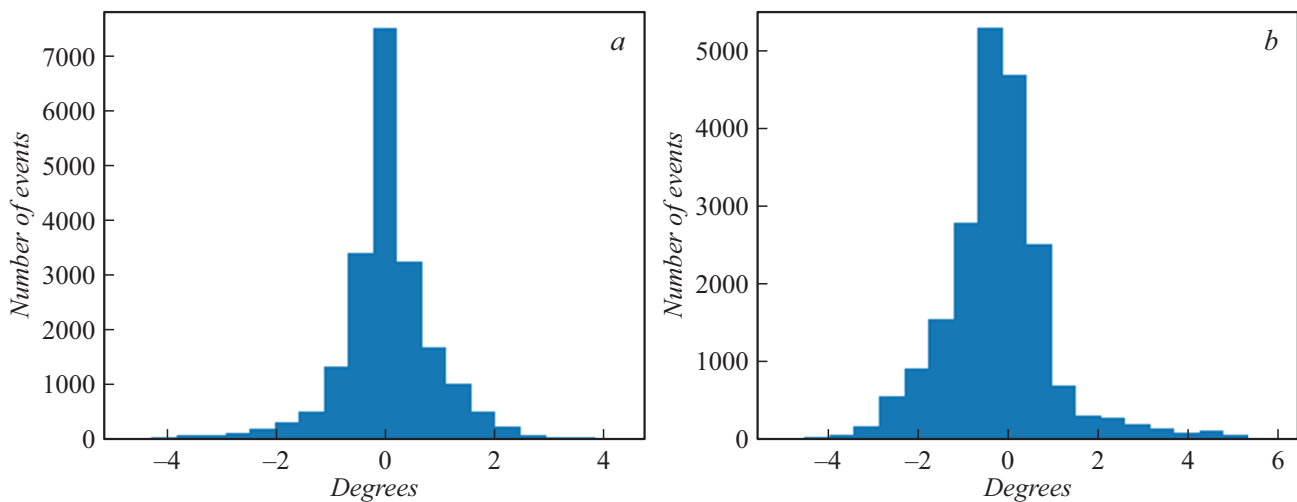


**Figure 4.** Errors of location angles (a) and azimuths (b) of the stars identified in the December 3, 2016 images

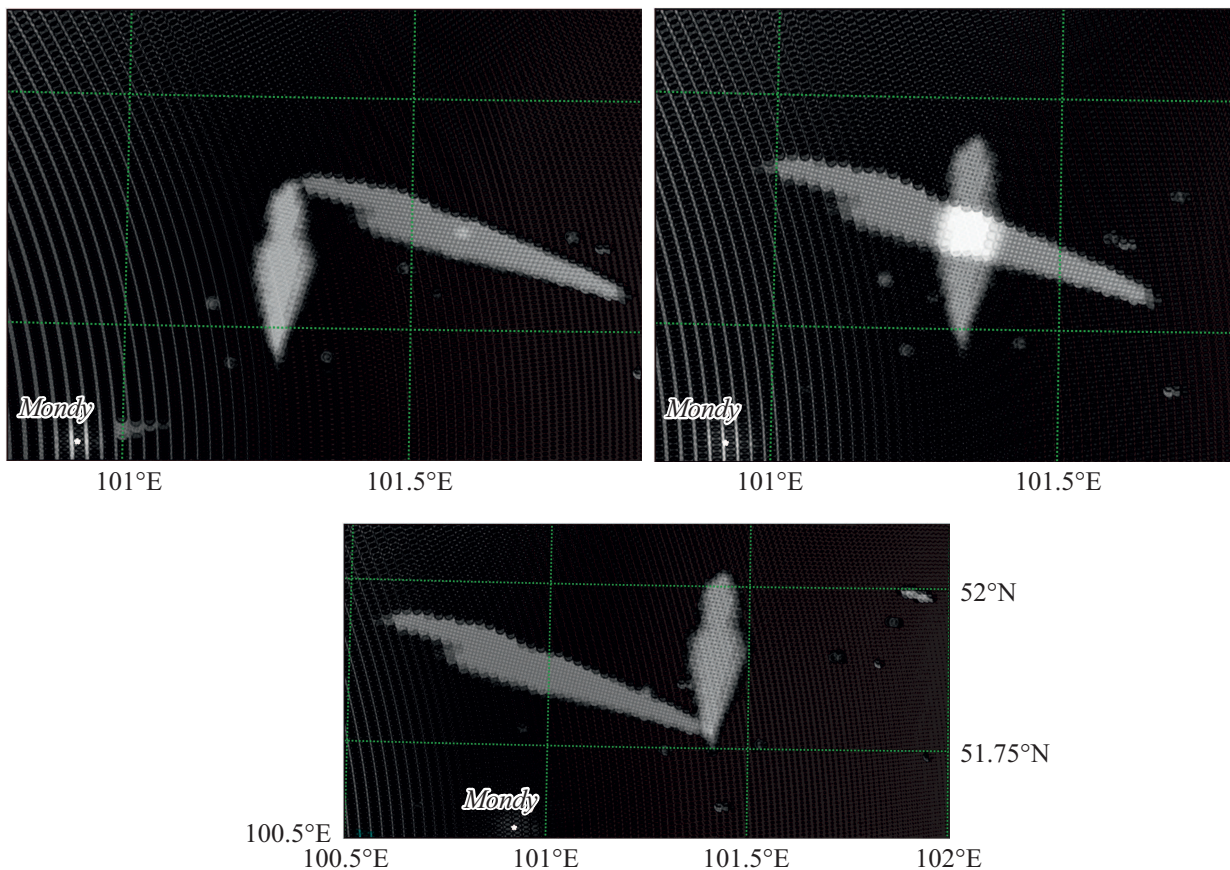


**Figure 5.** Projection of the meteor from KEO Sentinel and Allsky-340 cameras to the Earth's surface from heights of 78, 92 and 111 km, respectively. The map shows the observation point Mondy (Allsky-340), for which the observed event is near the zenith. The Tory observation point (KEO Sentinel) is off the map.

A similar analysis of the projection of the meteor trace showed that it was concentrated in the range  $\sim 88$ – $97$  km and propagated mainly in a southerly direction up to  $\sim 95$ – $106$  km. The eastward propagation of the trace occurred at an altitude of  $\sim 88$  km with an average velocity

of about 30 m/s. In the southerly direction, the trace propagated mainly at an altitude of about 94 km with an average velocity of about 84 m/s. In the westerly direction, the average speed of the trace was about 52 m/s. It should be noted that the velocities obtained from the optical

observations by the method described above were close to the ionization trace velocities obtained in [28] from the ionosonde data.

## Conclusion

The presented technique makes it possible to identify stars quite accurately on the frames of the wide-angle system, to obtain the spatial parameters of the registered events and to build the projections on the Earth's surface accordingly. The errors in determining the identified stars do not exceed  $0.8^\circ$ . The use of two or more cameras separated by some distance allows you to create a stereoscopic representation of different events, allowing a more complete assessment of the observed event. After processing the LLMT images with the presented algorithm, the following spatial characteristics of the trace were obtained: propagation heights — from 88 to 106 km ( $\pm 1.2$  km), propagation direction — predominantly southerly. Track speeds in the main directions were also calculated: southerly, westerly and easterly —  $\sim 84$ ,  $\sim 52$  and  $\sim 30$  m/s, respectively. This technique is expected to be used in the future to estimate the three-dimensional coordinates of objects observed with wide-angle optical systems, such as meteors, acoustic-gravity wave manifestations, etc.

## Funding

This work was financially supported by the Ministry of Education and Science of Russia (grant № 075-GZ/Ts3569/278) and the Russian Foundation for Basic Research № 19-35-90093.

## Conflict of interest

The authors declare that they have no conflict of interest.

## References

- [1] I.S. Izmailov, M.L. Khovrichева, M.Yu. Khovrichев, O.V. Kiyayeva, E.V. Khrutskaya, L.G. Romanenko, E.A. Roshchina, K. Maslennikov, O.A. Kalinichenko. *Astron. Lett.*, **36** (5), 349 (2010).
- [2] D. Lang, D.W. Hogg, K. Mierle, M. Blanton, S. Roweis. *Astron. J.*, **139** (5), 1782 (2010). DOI: 10.1088/0004-6256/139/5/1782.
- [3] T. Aso, T. Hashimoto, M. Abe, T. Ono, M. Ejiri. *J. Geomagn. Geoelectr.*, **42** (5), 579 (1990). <https://doi.org/10.5636/jgg.42.579>
- [4] D. Megan Gillies, D. Knudsen, E. Donovan, B. Jackel, R. Gillies, E. Spanswick. *J. Geophys. Res. Space Phys.*, **122**, 8181 (2017). DOI: 10.1002/2016JA023758
- [5] B.J. Jackel, F. Creutzberg, E.F. Donovan, L.L. Cogger. *Sodankylä Geophys. Observ. Publ.*, **92**, 97 (2003).
- [6] C. Störmer. *Comptes Rendus de l'Académie des Sciences*, **150**, 1631 (1910).
- [7] G. Witt. *Tellus*, **14** (1), 1 (1962). DOI: 10.3402/tellusa.v14i1.9524
- [8] G. Romick, A. Belon. *Planet. Space Sci.*, **15** (11), 1695 (1967). [https://doi.org/10.1016/0032-0633\(67\)90008-6](https://doi.org/10.1016/0032-0633(67)90008-6)
- [9] H.C. Stenback-Nielsen, T.J. Hallinan. *J. Geophys. Res.*, **84**, 3257 (1979). <https://doi.org/10.1029/JA084iA07p03257>
- [10] M.N. Kouahla, G. Moreels, M. Faivre, J. Clairemidi, J.W. Meriwether, G.A. Lehmacher, E. Vidal, O. Veliz. *Adv. Space Res.*, **45**, 260 (2010). <https://doi.org/10.1016/j.asr.2009.10.015>
- [11] T. Pedersen, B. Gustavsson, E. Mishin, E. MacKenzie, H.C. Carlson, M. Starks, T. Mills. *Geophys. Res. Lett.*, **36** (18), (2009). DOI: 10.1029/2009GL040047
- [12] A.V. Shindin, V.V. Klimenko, D.A. Kogogin, A.B. Beletsky, S.M. Grach, I.A. Nasyrov, E.N. Sergeev. *Radiophys. Quantum El.*, **60** (11), 849 (2018). DOI: 10.1007/s11141-018-9852-0
- [13] R. Danescu, F. Oniga, V. Turcu, O. Cristea. *Sensors*, **12**, 12940 (2012). DOI:10.3390/s121012940
- [14] S. Shah, J.K. Aggarwal. *Pattern Recogn.*, **29** (11), 1775 (1996). [https://doi.org/10.1016/0031-3203\(96\)00038-6](https://doi.org/10.1016/0031-3203(96)00038-6)
- [15] D. Barghini, D. Gardiol, A. Carbognani, S. Mancuso. *Astron. Astrophys.*, **626**, A105 (2019). <https://doi.org/10.1051/0004-6361/201935580>
- [16] J. Wang, F. Shi, J. Zhang, Y. Liu. *Pattern Recogn.*, **41** (2), 607 (2008). <https://doi.org/10.1016/j.patcog.2007.06.012>
- [17] F. Huang, Y. Wang, X. Shen, C. Lin, Y. Chen. *Appl. Opt.*, **51** (34), 8169 (2012). <https://doi.org/10.1364/AO.51.008169>
- [18] S.S. Beauchemin, R. Bajcsy. In: *Multi-Image Analysis. Lecture Notes in Computer Science*, ed. by R. Klette, G. Gimel'farb, T. Huang (Springer, Berlin, Heidelberg, 2001). [https://doi.org/10.1007/3-540-45134-X\\_1](https://doi.org/10.1007/3-540-45134-X_1)
- [19] Multidimensional Gaussian filter [Electronic source] Available at: [https://docs.scipy.org/doc/scipy/reference/generated/scipy.ndimage.gaussian\\_filter.html](https://docs.scipy.org/doc/scipy/reference/generated/scipy.ndimage.gaussian_filter.html)
- [20] C. Cepelcha. *Bull. Astron. Inst. Czech.*, **38**, 222 (1987).
- [21] J. Borovička, P. Spurný, J. Kečliková. *Astron. Astrophys. Suppl. Ser.*, **112**, 173 (1995).
- [22] S. Bannister, L. Boucheron, D. Voelz. *Publ. Astron. Soc. Pac.*, **125**, 1108 (2013).
- [23] J.J. Moré. In: *Numerical Analysis. Lecture Notes in Mathematics*, ed. by G.A. Watson (Springer, Berlin, Heidelberg, 1978), v. 630.
- [24] ephemeris 4.0.0.2 [Electronic source] Available at: <https://pypi.org/project/ephem/>
- [25] V.P. Morozov. *Course in Spheroidal Geodesy* (Nedra, Moscow, 1979)
- [26] Keo Sentinel Wide-Angle Monochromatic Imager [Electronic source] Available at: <http://atmos.iszf.irk.ru/ru/data/keo>
- [27] A.V. Mikhalev, A.B. Beletsky, R.V. Vasiliev, M.V. Eiselevich, K.I. Ivanov, E.S. Komarova, A.V. Podlesny, S.V. Podlesny, T.E. Syrenova. In the collection: *Collection of abstracts of the XVI All-Russian Open Conference Modern Problems of Earth Remote Sensing from Space* (Moscow, IKI RAN, 2018), p. 476. DOI 10.21046/2070-16DZZconf-2018a
- [28] A.V. Mikhalev, A.B. Beletsky, R.V. Vasiliev, M.V. Eiselevich, K.I. Ivanov, E.S. Komarova, A.V. Podlesny, S.V. Podlesny, T.E. Syrenova. *Solar-Terrestrial Physics*, **5** (3), 130 (2019). DOI: 10.12737/szf-53201913
- [29] K.I. Ivanov, E.S. Komarova, R.V. Vasiliev, M.V. Eiselevich, A.V. Mikhalev. *Solar-Terrestrial Physics*, **5** (1), 100 (2019). DOI: 10.12737/szf-51201911